Cohesive and electronic properties of ordered Li-Al intermetallic compounds

1994 J. Phys.: Condens. Matter 6 3389

(http://iopscience.iop.org/0953-8984/6/18/015)

J. Phys.: Condens. Matter 6 (1994) 3389–3402. Printed in the UK

Cohesive and electronic properties of ordered Li–Al intermetallic compounds

A Arya†, G P Das‡, H G Salunke‡ and S Banerjee†

† Metallurgy Division, Bhabha Atomic Research Centre, Bombay 400085, India

‡ Solid State Physics Division, Bhabha Atomic Research Centre, Bombay 400085, India

Received 24 September 1993, in final form 2 February 1994

Abstract. Self-consistent electronic structure calculations have been performed on ordered lithium–aluminium compounds using the tight-binding linear muffin-tin orbital (TBLMTO) method. The FCC-based ground-state superstructures (namely $L1_2$ and $L1_0$ structures) show some systematic trends in their cohesive and electronic properties, which are in reasonably good agreement with the available experimental data. We have also compared the density of states, band structures and total ground-state energies of equiatomic AlLi compounds, between the FCC-based $L1_0$ structure and the BCC-based B32 structure. While the former shows a two-dimensional metallic behaviour, the latter shows a resemblance to a tetrahedral-bonded covalent solid, and is more stable. After detailed comparison with some recent LAPW calculations, we conclude that the TBLMTO method can be used as an efficient and reasonably accurate first-principles tool for studying the phase stability and chemical bonding in ordered intermetallic compounds.

1. Introduction

The I–III intermetallic compounds of lithium and aluminium are commercially important, because of their low density, high elastic modulus and high strength-to-weight ratio, and hence these are suitable materials for aerospace applications [1, 2]. The equilibrium temperature–concentration phase diagram for Li–Al alloys and the corresponding thermodynamic data exist in the literature [3, 4]. Between the two terminal solid solutions (around FCC-Al and BCC-Li), there exists a number of intermediate phases, such as the stable AlLi phase (B32 structure) and the metastable Al_3Li phase ($L1_2$ structure). The equi-concentration AlLi (β) phase, for example, is a promising candidate as an anodic material in high-energy density batteries. The effect of Li addition is not only to make the compound lighter, but also to increase the values of the elastic constants of Li–Al alloys [5]; this is somewhat unexpected because the Young modulus of Li itself is one order of magnitude lower than that of Al. Significant improvements in the mechanical behaviour of these alloys have been achieved by rapid solidification, powder metallurgy processing [6]. In determining the mechanical properties of the alloy, the metastable Al-rich Al_3Li (α') phase plays a significant role [7] in precipitation hardening of commercial Li–Al alloys. However, accurate experimental determination of the equilibrium and metastable phase boundaries of Li–Al system encounters with some difficulties, and even if obtained large error bars are associated. Structural and mechanical properties of an intermetallic compound are closely linked to its electronic structure. Precise first-principles electronic structure calculations lead to a proper understanding of the structural competition between the various stable and metastable phases of Li–Al compounds. Furthermore, an accurate prediction of the stability sequence of the ordered compounds at zero temperature is an essential prerequisite for producing the *correct*

0953-8984/94/183389+14$19.50

first-principles phase diagram which require the additional entropy contribution to the free energy.

Density functional theory is now a well established tool for giving an accurate description of the electronic structures of solids [8,9]. The most widely used electronic structure methods for handling intermetallic compounds are (i) the linear muffin-tin orbital (LMTO) [10, 11], (ii) the augmented spherical wave (ASW) [12], and (iii) the linear augmented plane wave (LAPW) [10, 13] methods, which are nothing but the linearized versions of the most accurate partial-wave band structure methods (namely KKR and APW). Particularly relevant to the present discussion are the predictions of cohesive energy, compound formation energy and so on with reasonably good accuracy ($\leqslant 0.01$ eV per atom), and LAPW is presumably the most suitable (although most expensive) method for this purpose. On the other hand, the LMTO method, in conjunction with the atomic sphere approximation (ASA), is very fast and especially well suited for handling close-packed structures and complex systems like epitaxial interfaces, which can be described in terms of large supercells [14]. Such supercell treatment is also found to be convenient for first-principles theoretical investigations of ordered intermetallic compounds, whose various ground-state superstructures are well described in the literature [15, 16]. In this context, one of the crucial tests of an electronic band structure method is the correct prediction of the stability sequence of the different superstructures. First-principles calculations on a number of Li–Al compounds have been reported in the literature, using pseudopotential [17], LCAO [18, 19], LMTO [20, 21], LAPW [22–24] and ASW [25] methods. There is, however, disagreement between the results obtained for the same compound attacked by two different methods. Also lacking is a systematic investigation of the electronic and cohesive properties of *all possible* ordered superstructures of Li–Al intermetallics. We have therefore deployed the first-principles TBLMTO method (to be discussed in the next section), which is reasonably accurate and yet requires substantially less computer time compared to, say, the LAPW method. The method, as such, is applicable to any kind of ordered binary intermetallics. The Li–Al system should serve as an ideal test-case, since a significant amount of experimental data already exists on this system [2], in order to substantiate our calculated results. Although Al and Li are both simple metals (no d electrons), with nearly free electron-like valence bands, they are chemically rather different due to their atomic size, valency and electronegativity. Depending on composition (i.e. whether it is the Al-rich or the Li-rich side of the phase diagram) there will be sizable charge transfer and a varying degree of chemical bonding due to the effect of the local environment. Recently there have also been attempts to determine from first principles, the solid part of the Li–Al phase diagram [26, 27]. In order to determine the most stable structures, consistent with a given lattice (FCC, BCC and so on), using say the cluster variation method (CVM) [28], one must first compute the cohesive (or formation) energies of the pure metals as well as of their ordered compounds. These total energies can then be used to obtain the effective cluster interactions, by means of the Connolly–Williams method (CWM) [29].

In this paper we restrict ourselves only to $L1_2$ and $L1_0$ structures (figure 1) which are FCC-based ground-state superstructures under the nearest-neighbour pair approximation. The pure constituents, namely Al and Li, are both taken to be FCC in this case. For the sake of comparison of our LMTO total-energy differences with those obtained from LAPW calculations, as well as with the available experimental data, we have also included here the results of our calculation on BCC Li and on B32 : AlLi (figure 1(c)). The nature of chemical bonding in $L1_2$, $L1_0$ and B32 structures is quite different and can be correlated with the relative stability of the respective compounds. The paper is organized as follows. In section 2 we give a short description of the computational scheme that has been used.

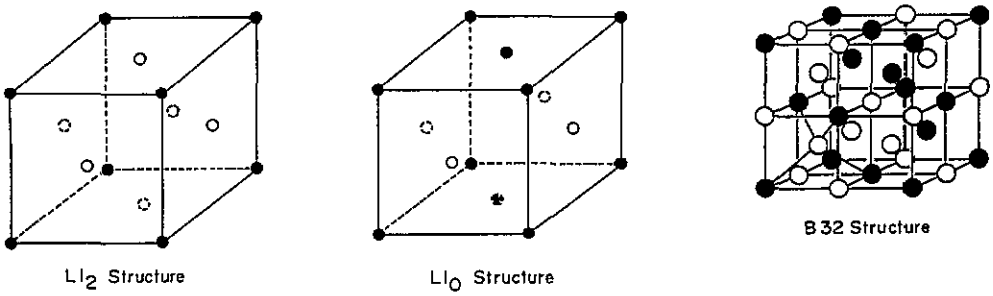

Figure 1. Crystal structures of $L1_2$, $L1_0$ and B32 phases of Li–Al intermetallic compound. The open circles denote A atoms and the full circles denote B atoms.

In section 3 we summarize the cohesive properties (the lattice constant, bulk modulus, cohesive energy, heat of formation and so on); we also present the results of our self-consistent calculations of the band structures, total and partial densities of states, charge transfer, and so on. Finally, in section 4, we summarize our conclusions.

2. Method and calculations

We have used the self-consistent scalar relativistic LMTO-ASA method and have included the so-called 'combined correction' terms. Here space is divided into muffin-tin spheres centred at various atomic sites R, such that the sum of the sphere volumes equals the volume of the unit cell. The potential is calculated using the density functional prescription under the local density approximation (LDA) [30, 31]. We use here the von Barth–Hedin parametrization [32] of the exchange-correlation potential. The LMTO–ASA method has the advantage of using the same type of (minimal) basis set for all the elements in the periodic table. It has been shown [33, 34] that the LMTO basis set may be transformed exactly into a short-range so-called *first-principles tight-binding basis*. The TBLMTO basis, unlike other semi-empirical tight-binding basis sets, is highly dependent on the environment and hence is sensitive to the different local chemical rearrangements of an underlying (say FCC) intermetallic lattice. The use of ASA and TB (or screened) representation makes the computation particularly fast on a computer for two reasons [14, 35]: (i) one requires a solution to an eigenvalue problem of size only 9×9 (for s, p, d electron elements) per atom at each point in reciprocal space, and (ii) the screened structure constant for each atom R needs only up to second-nearest neighbour atoms R'. The computer program used for the present calculation [36] has already been deployed for self-consistent calculations for s-, p-, d- and f-electron elements, and the corresponding potential parameters have been tabulated [37]. In our calculation, although s-, p- and d- partial waves have been used (i.e. maximum angular momentum $l_{max} = 2$), the d orbitals on both Li and Al sites have been *downfolded* [36]. It is worth noting at this point that we cannot afford to throw away the d orbitals altogether from the basis set expansion, because of the anisotropic bonding between the Al atoms strengthened by the fractional valence electrons donated by Li. Restricting the basis set to $l_{max} = 1$ for Li (as was done by Masudo-Jinda and Terakura in their ASW calculation [25] which might lead to incorrect trends in cohesive and elastic properties). This point has already been discussed by Guo and co-workers (see the appendix of [23]). That is why we have retained $l_{max} = 2$ but *downfolded* the d orbitals, thereby restricting the size of the Hamiltonian and overlap matrices, but without sacrificing the accuracy of

our results. This is a unique feature of the present TBLMTO–ASA method [36]. Finally, the tetrahedron method for the Brillouin zone (i.e. k-space) integrations has been used with its latest version, which avoids misweighting and corrects errors due to the linear approximation of the bands inside each tetrahedron [38, 39]. Fifteen equispaced k-points have been chosen along each direction of the cubic Brillouin zone, resulting in 120 irreducible k-points, say, for the FCC structure leading to k-converged calculations.

For the type of intermetallic systems treated here, one can ensure a reasonably small overlap between the atomic spheres without introducing any interstitial ('empty') spheres. In LMTO–ASA, the approximation due to spherical averaging is manageable, provided the overlap between the spheres, defined as $[100(s_1 + s_2 - d)/s_1]$, is less than 30%; here s_1 and s_2 ($s_1 \leqslant s_2$) are the radii of the two overlapping spheres and d is the distance between them. Incorporating the so-called 'combined correction', one can partly salvage the error due to spheridization of the potential and charge density. We have used the *same* Wigner–Seitz radius (s_{av}) for Al and Li in a particular structure, even though strictly speaking one should adjust the sphere radii (conserving the cell volume of course) which will ensure their approximate charge neutrality†. The self-consistent LMTO–ASA potentials from the ordered-phase calculation may even be used later for treating the disordered phases.

3. Results and discussion

3.1. Cohesive properties

By cohesive properties we mean the equilibrium lattice constants, bulk modulus, cohesive energies, heats of formation and so on. All these quantities are related to the *total ground-state energy*, which is one of the most fundamental quantities coming out of a self-consistent electronic structure calculation. The volume-dependent total energies for any system should ideally fall on a parabola, whose minimum (i.e. first derivative) yields the equilibrium volume and hence the equilibrium lattice constant (for cubic systems). The bulk modulus is related to the second derivative of the total energy with respect to the volume:

$$B = V_0(\mathrm{d}^2E/\mathrm{d}V^2) \tag{1}$$

and its calculated values often have rather large error bars. Table 1 shows our LMTO results for the equilibrium volume, lattice constant and bulk modulus obtained for FCC : Al, $L1_2$: Al_3Li, $L1_0$: AlLi, $L1_2$: $AlLi_3$, FCC : Li, BCC : Li and B32 : AlLi. In the Li–Al system, one sees strong deviations of the alloy volume from the linearly interpolated volume of Vegard's law. For pure Li, the equilibrium volume per atom is $\sim 25\%$ larger, while its bulk modulus is a factor of six lower compared to that of pure Al. With increasing Li composition, however, the volume shrinks and simultaneously the bulk modulus decreases. The calculated values of equilibrium volumes (hence lattice parameters) and bulk moduli for the pure constituents as well as the compounds follow the same trend. Our calculated lattice constants are only $\sim$ 1–4% smaller than experimental results [40, 41] (the maximum discrepancy is $\sim 4\%$ for pure Li), and our calculated bulk moduli (which are more likely to have large errors) are in surprisingly good agreement with experimental results (available only for FCC-Al, BCC-Li [41] and $L1_2$: Al_3Li [2]. On the other hand, the numbers coming out of the presumably more precise full-potential LAPW calculations are by no means in

† For example, we have found for B32: LiAl, $s_{Li}/s_{av} = 0.95$ and $s_{Al}/s_{av} = 1.045$ yields neutral Li and Al spheres, in conformity with the results of [20].

better agreement with experiment, but these show exactly the same trend as our TBLMTO–ASA results. Although this may seems to be apparently fortuitous, we are inclined to attribute it to the fact that all these ordered intermetallic compounds are rather close-packed and do not need any artificial 'empty spheres' for the purpose of satisfying the ASA requirements. But one must be cautious while making such comparisons. Firstly, reliable experimental numbers are available only for stable elements or compounds (like B32 : LiAl); for metastable compounds (like $L1_2$: Li_3Al) it is difficult to get precise measurements of lattice parameters. Secondly, even for a stable stoichiometric compound like the B32 : LiAl, the formation of vacancies and antisite atoms make the so-called *'defect-phase' more stable* [20].

Table 1. Cohesive properties of lithium–aluminium compounds. The three values indicated in each section correspond to results obtained from the present LMTO calculation (row 1), the LAPW calculations of Guo and co-workers [22–24] (row 2) and the experimental values at room temperature [2, 40–43] (row 3). Units used are as follows. Lattice constant 1 Å = 1.889 727 au; equilibrium volume 1 $cm^3\,mol^{-1}$ = 11.204 338 au^3 per atom; bulk modulus 1 GPa = 10 kbar; cohesive energy and formation energy 1 $kJ\,mol^{-1}$ = 0.762 mRy per atom.

		Al (FCC)	Al_3Li (L12)	AlLi ($L1_0$)	$AlLi_3$ (L12)	Li (FCC)	Li (BCC)	AlLi (B32)
Equilibrium	(1)	9.6250	9.5498	9.3323	10.1517	11.2294	11.5268	9.2568
Volume	(2)	9.5570	9.4585	9.2805	9.7403	11.4241	11.4387	9.2148
($cm^3\,mol^{-1}$)	(3)	9.9745[f]	9.7092[f]	——	——	12.9043[f]	12.9903[f]	9.7229[f]
Lattice	(1)	3.9984	3.9879	3.9574	4.0700	4.2092	3.3701	6.2650
Constant	(2)	3.9889	3.9750	3.9501	4.0143	4.2334	3.3615	6.2555
(Å)	(3)	4.0462[a]	4.0100[a]	——	——	4.4089[b]	3.5071[b]	6.3685[a]
Bulk	(1)	76.80	68.93	61.57	30.80	19.03	12.02	78.96
Modulus	(2)	82.20	72.00	50.41	28.37	13.64	15.25	57.75
(GPa)	(3)	75.20[b]	66.00[c]	——	——	——	12.00[b]	——
E_{coh}	(1)	−405.798	−366.150	−318.191	−261.589	−207.624	−206.789	−330.079
($kJ\,mol^{-1}$)	(2)	−387.16	−342.30	−288.77	−225.91	−164.11	−163.45	−297.17
	(3)	−322.4[b]	——	——	——	——	−161.1[b]	——
E_{form}	(1)	0.000	−9.896	−11.48	−4.422	0.000	0.835	−26.29
($kJ\,mol^{-1}$)	(2)	0.000	−10.90	−13.13	−6.04	0.00	0.656	−22.40
	(3)	——	——	——	——	——	−1.214[e]	−24.30[d]

[a] Experimental data taken from [40].
[b] Experimental data taken from [41].
[c] Experimental data taken from [2].
[d] Experimental data taken from [42].
[e] Experimental data taken from [43].
[f] Calculated from experimental lattice constant.

The cohesive energy E_{coh} is defined as the difference between the total ground-state energy of the solid state and the sum total of the energies of the individual isolated atoms weighted by their respective fractional concentrations. The self-consistent free-atom calculations have been performed semi-relativistically with a large cutoff (r_{max} = 30 au) [36]. The formation energy E_{form} of a FCC-based compound A_cB_{1-c} is obtained by subtracting from its cohesive energy the weighted sum of the cohesive energies of the constituent FCC metals:

$$E_{form}(A_cB_{1-c}) = E_{coh}(A_cB_{1-c}) - [cE_{coh}^{FCC}(A) + (1-c)E_{coh}^{FCC}(B)]. \qquad (2)$$

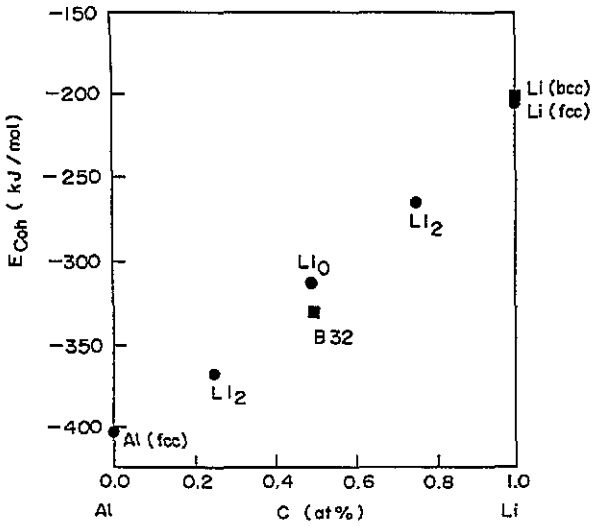

Figure 2. Calculated cohesive energies of Li–Al compounds as a function of composition. All the structures except BCC-Li and B32 : AlLi are FCC-based.

Our calculated E_{coh} and E_{form} values (table 1) are compared with the corresponding LAPW numbers and also with the available experimental data. The free-atom energies used in our calculation are −483.985 Ry and −14.771 Ry for Al and Li respectively, which differ from the numbers used in LAPW calculation [23], namely −483.547 for Al and −14.665 for Li. The subtle differences in the manner in which atomic calculations are performed are reflected in the systematic overestimate in our E_{coh} values (table 1 and figure 2). Another plausible reason for this overestimate is the shape approximation in ASA, which replaces the exact non-spherical charge density $n(r)$ (appearing in the expression for the total energy functional), by its spherical part $n(r)$ [14, 35]. These systematic errors in E_{coh}, however, get cancelled while calculating E_{form} (via relation (2)), which show fairly good agreement with the corresponding LAPW results [22–24]. As a function of concentration, E_{form} shows a V-shape curve (figure 3), with a minimum at the equi-concentration AlLi compound, in conformity with the LAPW result [27]. Unfortunately, very few experimental thermochemical data exist on this family of compounds [42]. The B32 structure has a larger formation energy compared to the $L1_0$ structure, making the former thermodynamically more stable. In fact, the experimental value of formation energy (24.3 kJ mol^{-1}) [42] is very close to our calculated value (26.29 kJ mol^{-1}) for the B32 structure, which is $\sim$ 15 kJ mol^{-1} higher than that of the $L1_0$ structure. This feature will be further clarified on the basis of a bonding argument in the next section. Another notable feature is that the cohesive energies of the FCC and BCC phases of Li are nearly the same and the difference $\Delta E = E_{coh}^{BCC} - E_{coh}^{FCC}$ (which we have tabulated as the formation energy for the BCC phase) turns out to be *positive*, which agrees with the LAPW result [24] in sign as well as in magnitude. The structural energy difference predicted with phase-diagram fitting [43] gives a wrong sign and hence does not describe the behaviour of Li, as was pointed out by Sluiter and co-workers [27]. Our conclusion supports the fact that at zero temperature, the BCC form becomes unstable in favour of FCC. Indeed, it has recently been verified by inelastic neutron scattering studies [44], that Li undergoes a martensitic phase transformation from BCC to a twinned FCC-based 9R superstructure (Sm type) below $\sim$ 78 K, and as temperature increases the BCC form becomes stable by merit of its large vibrational entropy.

3.2. *Effective cluster interaction (ECI)*

The volume-dependent ECI for the Li–Al system, based upon an FCC parent lattice, have been

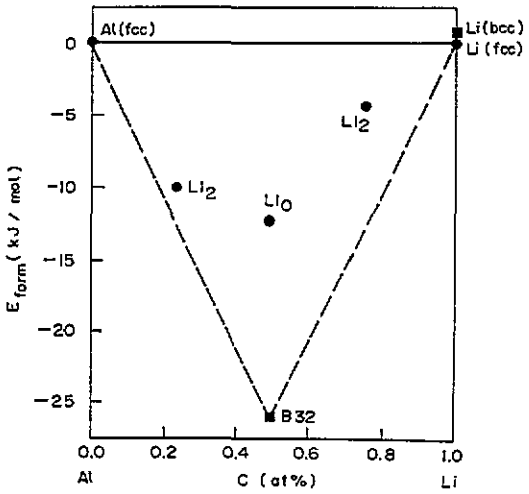

Figure 3. Calculated formation energies of Li–Al compounds as a function of composition. All the structures except BCC-Li and B32 : AlLi are FCC-based. B32 structure is most stable.

Table 2. Effective (multisite) interaction coefficients (J_γ) for an FCC lattice under the tetrahedron approximation. Successive clusters ($\gamma = 0, 1, \ldots, 4$) correspond, respectively, to empty (0), a point (1), a NN pair (2), a triangle containing NN pairs only (3), and a tetrahedron (4). The units for the calculation of J_γ are kJ mol^{-1} (see text).

γ	$J_\gamma^{(0)}$	$J_\gamma^{(1)}$	$J_\gamma^{(2)}$
0	−55.70	−54.01	2.82
1	50.25	−33.51	1.83
2	−28.20	10.24	−0.66
3	−17.98	4.62	−0.26
4	15.41	−4.14	0.25

determined under *nearest-neighbour* pair approximation, using (CWM). The CWM is based on a formal expression for the total energy of a particular configuration (superstructure) Ψ as

$$E_{\mathrm{coh}}^{\Psi}(V) = \sum_{\gamma=0}^{\gamma_{\max}} J_\gamma(V)\xi_\gamma^{\Psi} \tag{3}$$

where the sum runs over all the cluster up to the maximum of a tetrahedron in this case, $J_\gamma(V)$ are the volume-dependent ECI for the cluster γ, and the ξ_γ are the corresponding cluster correlation functions. The J_γ have been calculated by inverting the above equation (3) to give

$$J_\gamma(V) = \sum_{\Psi} (\xi_\gamma^{\Psi})^{-1} E_{\mathrm{coh}}^{\Psi}(V) \tag{4}$$

where the sum is over all the FCC-based ground-state superstructures. By expanding the cohesive energies around the equilibrium volume V_0, and retaining terms up to second order, we get the volume dependence of the ECI as

$$J_\gamma(V) = J_\gamma^{(0)} + J_\gamma^{(1)} V + J_\gamma^{(2)} V^2. \tag{5}$$

Table 2 summarizes the calculated coefficients for the volume expansion of ECI for FCC lattice. These ECI, which are averaged over all the possible ground-state superstructures indeed reproduce the cohesive energies of the superstructures which were originally obtained from our LDA. This establishes the feasibility of using our TBLMTO method, in conjunction with CWM for obtaining the ECI.

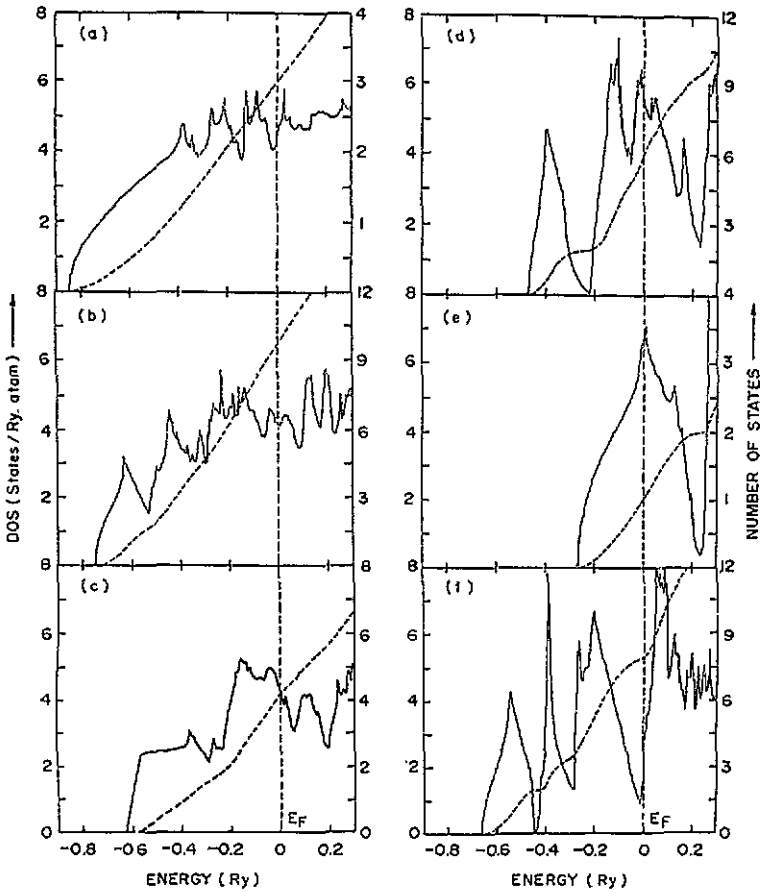

Figure 4. Density of states in (*a*) Al (FCC), (*b*) Al_3Li (L12), (*c*) AlLi (L10) (*d*) $AlLi_3$ (L12) (*e*) Li (FCC) and (*f*) AlLi (B32). The total DOS (full curves) have been divided by the number of basis atoms, so that each figure shows the average contribution per Ry per atom. The corresponding NOS (broken curves) shows from its intercept with E_F, the total valence charge (see table 4).

3.3. Electronic structure

All results in this subsection correspond to the equilibrium lattice constant of the respective structures (as determined in section 3.1, table 1). Figures 4 and 5 show the total and corresponding site-projected DOS of the FCC based superstructures and of B32 : LiAl. Superposed onto the DOS is the integrated quantity called the 'number of states' (NOS), whose cutoff at the Fermi energy yields the fractional band occupancy. Corresponding band structures along the high symmetry directions are shown in figure 6. Because of the close similarity of the cohesive and electronic properties between BCC-Li and FCC-Li (see the discussion in section 3.1), we have included (in figures 4–6) our results only for FCC-Li. However, the DOS and bands for BCC-Li and FCC-Al compare quite well with the KKR results of Moruzzi and co-workers [45]. Most of the gross features in the electronic structures of Li–Al compounds can be seen in the DOS, which in the present case are mainly governed by s- and p-electrons of Li and Al. For pure Al, the DOS resembles a free-electron parabola, as expected. For $L1_2$: Al_3Li the occupied DOS more or less resembles that of pure Al, excepting some hybridization effects causing a dip at around −0.5 Ry. For $L1_0$: AlLi, the

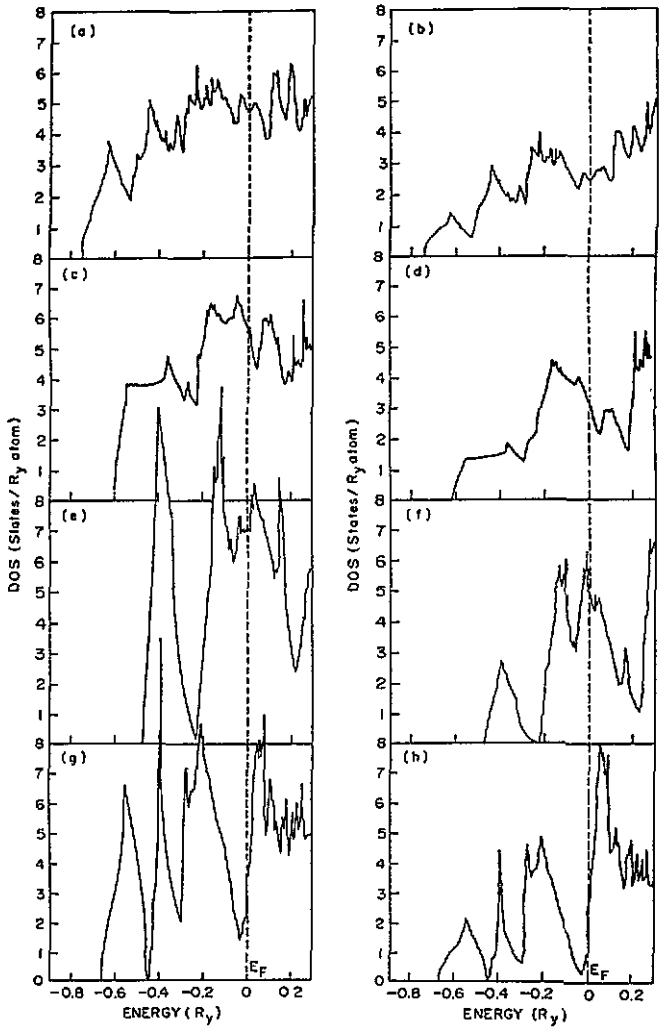

Figure 5. Partial DOS projected onto Al- and Li-sites respectively, for $L1_2$: Al_3Li (*a*) and (*b*), $L1_0$: AlLi (*c*) and (*d*), $L1_2$: $AlLi_3$ (*e*) and (*f*), and B32 : AlLi (*g*) and (*h*). Note that each *of these partial DOS correspond to that of one full Li or Al atom, as embedded in the respective* compounds, so that the total area under the occupied part yields the fractional number of band electrons within the sphere (as given in table 4).

DOS below E_F shows a 'staircase' like structure with two nearly flat-topped 'steps'. This is characteristic of a two-dimensional structure formed by alternate planes of Al atoms and Li atoms [22] (see figure 1(*b*)). For the Li rich $L1_2$: $AlLi_3$, the s-like and p-like states are almost completely separated, causing the DOS to become almost zero at ~ -0.2 Ry between the two distinct humps. This is also reflected in the flat plateau in the NOS. Finally in FCC-Li, the picture boils down to a single s-peak.

A few subtle differences between the electronic structures of these compounds emerge from their band dispersions (figure 6). Comparison with published band structures of these compounds, as well as of the pure constituents, show reasonably good agreement, as expected. The threefold-degenerate Γ_{25} levels are occupied in Al_3Li and AlLi, but

get pushed above E_F in $AlLi_3$. This signifies weaker bonding in $AlLi_3$ and hence lower E_{form}. In the case of $L1_0$: AlLi, the pronounced two-dimensional behaviour (in Al planes) gets reflected in the weak band dispersion along the AM direction (figure 6(*c*)) which is perpendicular to the Al plane. At the X point, the two lowest bands are non-degenerate, which demonstrates the non-negligible interaction between the Al and Li planes [22]. The dip at ~ 0.5 Ry in the DOS of $L1_2$: Al_3Li originates from the opening up of a hybridization gap at the X point between the lowest s-like and the p-like bands (figure 6(*b*)). Some of the key electronic parameters emerging out of our calculations are summarized in table 3. For example, the DOS at the Fermi level, $N(E_F)$, is an important quantity carrying information about the stability of the structure; it is also directly related (via electron–phonon coupling constant), to the electronic specific heat and superconducting transition temperature. Our calculation reveals $N(E_F)$ to be a minimum for the Al_3Li, and increases with the increase of Li concentration. Focusing on the structure of the DOS at the Fermi level, we see only Al_3Li has a local minimum at E_F, while for both AlLi and $AlLi_3$, E_F lie on the 'falling edge'. This can be correlated with the fact that the former compound is (meta)stable, while the latter two are unstable with respect to the corresponding BCC-based competing structures [22–24].

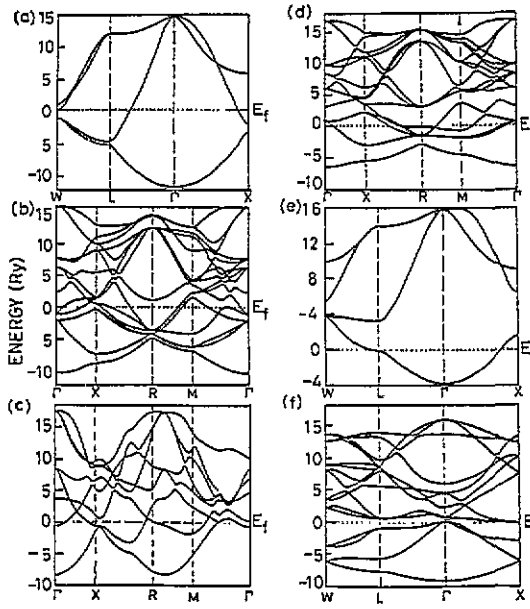

Figure 6. Self-consistent band structures, along high symmetry directions, of the different phases of Li–Al compounds (same sequence as in figure 4). The Fermi level is indicated by E_F.

The characteristic energies of the s- and p-bands are given in LMTO by the corresponding C and Δ parameters, which are respectively related to the band-centre and band-width hybridization [35]. The C values are seen to be progressively increasing as we move from the Al-rich to the Li-rich end, and simultaneously Δ goes down (see table 3). The width of the *occupied* band (W_{occ}) is simply obtained by subtracting from E_F, the lowest occupied eigenvalue (Γ_1 in this case). W_{occ} monotonically decreases with increasing Li concentration. For pure elements (FCC-Al and BCC-Li), we can compare our values of W_{occ} and $N(E_F)$ with the available KKR results [45] and the match is quite satisfactory.

The B32 : LiAl is the only compound for which a number of different band calculations have already been published [17–22]. This structure is not only stable compared to the $L1_0$ structure, but also has the minimum formation energy (see table 1 and figure 3) amongst

all the Li–Al compounds. Our calculated DOS and bands of the B32 structure are in perfect agreement with most of the earlier calculations [17–22], although there are subtle differences with the LCAO calculation of Zunger [18]. The three-humped DOS of the B32 structure (figure 4(f)) resembles that of a typical covalent-bonded diamond structure. The partial DOS projected onto Li and Al sites (figures 5(g) and 5(h)) are roughly similar to each other. The occupied part of the DOS can be broken up into three regions. The lowest-energy bonding peak is predominantly Al-s component, while the broad peak just below E_F is due to Al-p and Li-p. The sharp middle peak arises from sp antibonding states. Our result shows that E_F is situated on a steeply rising part of the DOS just above a minimum in the valley, in conformity with the earlier LMTO and LAPW calculations [20–22], but in contrast to the LCAO results of Zunger [19]. This exact location of E_F is crucial in LiAl because of its sensitivity to the vacancy-induced electronic instability. The charge density contours obtained by Guo and co-workers [22] clearly show that the Li–Al bonds in B32 structure are weakly covalent with a stronger polarization towards the Al sites. In sharp contrast, the $L1_0$: LiAl shows all signatures of a metallic bonding with a high (nearly double that of B32 structure) DOS at E_F. So it is quite expected that the B32 structure has a stronger and directional bond, as compared to those of $L1_0$ structure. This results in a higher E_{coh} as well as E_{form} for the B32 structure, as was seen in section 3.1 (table 1).

Table 3. Some important electronic parameters for lithium–aluminium compounds from a self-consistent LMTO calculation. (a) DOS at the Fermi level $N(E_F)$ in units of states per Ry per atom, (b) width of occupied band W_{occ}, (c) band-centre parameter C_{Rl} (measured with respect to E_F) and (d) band width parameter Δ_{Rl}. All the energy units used here are Rydberg.

Structure	$N(E_F)$ (Ry atom)$^{-1}$	W_{occ} (Ry)	Potential parameters (C and Δ) in Ry							
			Al				Li			
			C_s	Δ_s	C_p	Δ_p	C_s	Δ_s	C_p	Δ_p
Al (FCC)	4.187	0.86	−0.5773	0.118	0.1595	0.104	——	——	——	——
Al_3Li ($L1_2$)	4.167	0.74	−0.5489	0.118	0.1894	0.104	−0.0050	0.152	0.4745	0.111
AlLi ($L1_0$)	4.266	0.62	−0.5182	0.119	0.2285	0.104	0.0434	0.154	0.5183	0.111
$AlLi_3$ ($L1_2$)	5.953	0.47	−0.4963	0.109	0.2145	0.094	0.0490	0.141	0.5038	0.102
Li (FCC)	6.634	0.27	——	——	——	——	0.0309	0.128	0.4608	0.091
Li (BCC)	6.600	0.27	——	——	——	——	0.0240	0.124	0.4500	0.089
AlLi (B32)	1.971	0.69	−0.6255	0.122	0.1272	0.106	−0.0812	0.154	0.3926	0.111

In table 4 we summarize the fractional occupancies on Al and Li sites partitioned amongst various orbitals. Since these numbers generated from our ASA calculation represent charges within the overlapping atomic spheres, these should not be directly used to explain the inter-site charge transfer. The 'tail' of the Al orbital, for example, protrudes into the neighbouring Li sphere, whose size has been chosen to be same as that of the Al sphere (and hence relatively large). This results in a significant Al-like contribution to the Li-sphere charge, which is found to increase with increasing Al concentration (table 4), reaching a maximum value (1.496) in Al_3Li. However, since we have used the same WS sphere radii around both Al and Li sites, it should be possible to estimate the intra-site promotion of electrons and also the relative trend in the inter-site (or more appropriately *inter-sphere*) charge transfer. For example, if we compare the numbers for AlLi in $L1_0$ and B32 structures, we observe that more charge is transferred from the Li to Al sphere in the B32 structure; and it is this extra charge (~ 0.133 electrons) which goes in between the Al bonds, resulting in a strengthening of Al–Al bonds in a B32 structure. In other compounds, this inter-sphere

Table 4. The number of valence electrons (Q_t) inside the atomic (WS) spheres, partitioned according to angular momentum. The Q_{sph} are nothing but the fractional number of electrons inside the Al and the Li spheres, as embedded in the respective compounds, and are proportional to the total area under the occupied parts of the partial DOS (figure 5). The weighted sum of these sphere charges yields the total valence charge in the compound.

Structure	Total valence charge	Al				Li			
		Q_s	Q_p	Q_d	Q_{sph}	Q_s	Q_p	Q_d	Q_{sph}
Al (FCC)	3	1.104	1.476	0.420	3.0	——	——	——	——
Al_3Li ($L1_2$)	10	1.118	1.444	0.268	2.830	0.421	0.832	0.257	1.510
AlLi ($L1_0$)	4	1.129	1.344	0.151	2.624	0.424	0.802	0.150	1.376
$AlLi_3$ ($L1_2$)	6	1.231	1.213	0.064	2.508	0.451	0.631	0.082	1.164
Li (FCC)	1	——	——	——	——	0.492	0.478	0.031	1.001
Li (BCC)	1	——	——	——	——	0.498	0.471	0.031	1.000
AlLi (B32)	4	1.064	1.541	0.151	2.756	0.378	0.709	0.156	1.243

charge transfer is much less. The intra-atomic charge redistribution, mainly promotion from s to p electrons in both the Li and Al sites, can be observed in all the compounds, and is again most prominent in the B32 : AlLi, followed by that in $L1_2$: Al_3Li. These are, incidentally, the two most stable/metastable ordered structures that have been realized.

4. Summary

We have performed a first-principles investigation of the ordered binary compounds of lithium and aluminium using a self-consistent TBLMTO–ASA method. The systematic trends in electronic and cohesive properties of the FCC-based ground-state superstructures (namely $L1_2$ and $L1_0$ structures) are found to be in excellent agreement with experiment as well as with the more expensive LAPW calculations. For comparing the relative stability and the nature of chemical bonding between two competing structures with the same constituent concentration, we have also performed calculations on the BCC-based B32 : AlLi, which is known to be the most stable of all Li–Al compounds. The salient features that have emerged from our studies can be summarized as follows.

(i) The calculated lattice constants follow the same trend as the experimental and the existing LAPW results; in fact, our absolute numbers are in better agreement with experiment, as discussed in section 3. There is a systematic underestimate of the theoretical values, and the relative error varies between 1% (for pure Al) and 4% (for pure Li). The possible reasons for this consistent underestimate are first, zero-point vibrations (which are more predominant for lighter elements) are neglected here; second, these are zero-temperature calculations and the temperature variation of lattice parameters must be taken into account before comparing with experimental numbers; third, LDA is traditionally believed to overestimate bonding.

(ii) The elastic behaviour of Li–Al alloys is rather unusual in the sense that there is an increase in the Young modulus and a simultaneous decrease of the bulk modulus, with increasing Li concentration [2, 5]. Our calculated bulk moduli decrease monotonically with increasing Li concentration, which is supported by the available experimental data (see table 1). However, in the literature [23, 25], there are conflicting interpretations of the theoretical results on the bulk modulus. It is worthwhile making a comparison of the cohesive properties of a typical compound, say Al_3Li, obtained using different LDA calculation schemes, namely LAPW [23], ASW [25] and the present TBLMTO schemes. The equilibrium lattice constants are 3.9752 Å, 3.9286 Å and 3.9879 Å respectively (the

experimental value is 4.01 Å), while the corresponding bulk moduli are 72 GPa, 96 GPa and 69 GPa respectively (the experimental value is 66 GPa)†. As can be seen, our TBLMTO results are in close agreement with the LAPW results (and also with experiment), but *not* with the ASW results. It should be noted that the reverse trend in the bulk modulus obtained in theASW calculation [25] is only for low Li-concentrations ($\leqslant$ 25 at.%), and the authors themselves have mentioned the ambiguity in their interpretations. In order to resolve this, Guo and co-workers have put forward some arguments (see the appendix of [23]), which is in conformity with our results.

(iii) Our calculated E_{coh} values show the same trend as those obtained from LAPW calculations, although the absolute values are overestimated, for reasons discussed in section 3.1. These E_{coh} values have been directly used in conjunction with the Connolly–Williams prescription in order to obtain the effective multisite interactions $J_\gamma(V)$ (see table 2). The cancellation of the systematic errors in E_{coh} is evident from the behaviour of compound formation energies (E_{form}), which not only yields the same V-shape concentration dependence of E_{form} (figure 3) as obtained from LAPW studies [27], but also reproduces quite accurately the experimental results like E_{form} for B32 : AlLi, the stability of FCC-Li at 0 K, and so on.

(iv) The magnitude of the Fermi level state density $N(E_F)$ as well as the exact location of E_F in the DOS bears the signature of the relative stability of an ordered compound. Our results show that $N(E_F)$ is a minimum (with E_F close to a valley) for the B32 structure, which has maximum stability. Amongst the FCC-based compounds, $N(E_F)$ is lowest for $L1_2$: Al_3Li. Both for $L1_0$: AlLi and $L1_2$: $AlLi_3$, E_F cuts through the falling edge of a peak in the DOS, while for $L1_2$: Al_3Li, it sits right inside a local minimum (figure 4(*b*)). This explains why $L1_2$: Al_3Li is the only metastable FCC-based structure encountered in precipitation-hardening treatment.

(v) A comparison of the cohesive and electronic properties of B32 and $L1_0$ structures reveals the difference in the nature of chemical bonding between the two. While the $L1_0$ structure shows a two-dimensional free-electron-like metallic behaviour, the B32 structure behaves like a 'covalent metal' with significant charge concentration along the Li–Al bond. The latter has a tendency to form tetrahedral diamond-like sp^3 bonds, characterized by a small inter-site transfer of charge from Li to Al, but a large intra-site promotion from s to p electrons.

In conclusion, we have shown that TBLMTO–ASA is an efficient and reasonably accurate first-principles calculational tool for investigating the structural stability (at zero temperature) and other microscopic details of the cohesive and electronic properties of ordered binary compounds. The results obtained here for Li–Al compounds are quite satisfactory. More calculations on both FCC- and BCC-based ground-state superstructures, with second-nearest-neighbour pair approximation, should be performed in order to determine the complete Li–Al phase diagram from first principles.

Acknowledgments

This work forms part of a PhD project carried out at the Indian Institute of Technology,

† In the appendix of [23], Guo and co-workers reported the results of two of their LMTO–ASA calculations for $L1_2$: Al_3Li, with the sphere radii of Al and Li as used in the ASW calculation of [25]. They obtained the lattice constant and bulk modulus respectively to 3.9434 Å and 68 GPa (with $l_{max} = 2$ for both Al and Li) and 3.9940 Å and 76 GPa (with $l_{max} = 1$ for Li and $l_{max} = 2$ for Al). Comparing the former calculation with ours (also with $l_{max} = 2$ but with d-orbitals downfolded), we find that the bulk modulus matches exactly, but surprisingly not the lattice constant.

Bombay, by one of the authors (AA), who is thankful to Professor M J Patni for his guidance and encouragement.

References

[1] Sanders T H Jr and Starke E A Jr (eds) 1981 *Aluminium–Lithium Alloys* (New York: Metall. Soc. AIME)
[2] Mueller W, Bubeck E and Gerold V 1986 *Proc. 3rd Int. Conf. on Al–Li Alloys* ed C Baker, P J Gregson, S J Harris and C J Peel (London: TMS-AIME) p 435
[3] McAlister A J 1982 *Bull. Alloy Phase Diagr.* **3** 177
[4] Murray J L 1988 *ALTC Division Report 5688-EA4* Alcoa Laboratories
[5] Noble B, Harris S J and Dinsdale K 1982 *J. Mater. Sci.* **17** 461
[6] Lavernia E J and Grant N J 1987 *J. Mater. Sci.* **22** 1521
[7] Simmons J P 1992 *PhD thesis*
[8] Lundqvist S and March N H 1983 *Theory of the Inhomogeneous Electron Gas* (New York: Plenum)
[9] Jones R O and Gunnarsson O 1989 *Rev. Mod. Phys.* **61** 689
[10] Andersen O K 1975 *Phys. Rev.* B **12** 3060
[11] Skriver H L 1984 *The LMTO Method* (Berlin: Springer)
[12] Williams A R, Kubler J and Gelatt C D 1979 *Phys. Rev.* B **19** 6094
[13] Jansen H J F and Freeman A J 1984 *Phys. Rev.* B **30** 561
[14] Das G P 1992 *Pramana–J. Phys.* **38** 545
[15] Richards M S and Cahn J W 1971 *Acta Metall.* **19** 1263
[16] Ferro R and Saccone A 1993 *Materials Science and Technology: Structure of Solids, vol 1* ed R W Cahn, P Hassen and E J Kramer (Weinheim: VCH) p 123
[17] Lu D and Carlson A E 1989 *Phys. Rev.* B **40** 980
[18] Zunger A 1978 *Phys. Rev.* B **17** 2582
[19] Hafner and Weber 1986 *Phys. Rev.* **33** 747
[20] Asada T, Jarlborg T and Freeman A J 1981 *Phys. Rev.* B **24** 510
[21] Christensen N E 1985 *Phys. Rev.* B **32** 207
[22] Guo X Q, Podloucky R and Freeman A J 1989 *Phys. Rev.* B **40** 2793
[23] Guo X Q, Podloucky R and Freeman A J 1990 *Phys. Rev.* B **41** 12432
[24] Guo X Q, Podloucky R and Freeman A J 1990 *Phys. Rev.* B **42** 10912
[25] Masuda-Jindo K I and Terakura K 1989 *Phys. Rev.* B **39** 7509
[26] Podloucky R, Jansen H J F, Guo X Q and Freeman A J 1988 *Phys. Rev.* B **37** 5478
[27] Sluiter M, de Fontaine D, Guo X Q, Podloucky R and Freeman A J 1990 *Phys. Rev.* B **42** 10460
[28] Kikuchi R 1951 *Phys. Rev.* **81** 988
[29] Connolly W and Williams A R 1983 *Phys. Rev.* B **27** 5169
[30] Hohenberg P and Kohn W 1964 *Phys. Rev.* **136** B864
[31] Kohn W and Sham L J 1965 *Phys. Rev.* **140** A1133
[32] Hedin L and Lundqvist B I 1971 *J. Phys. C: Solid State Phys.* **4** 2064
[33] Andersen O K and Jepsen O 1984 *Phys. Rev. Lett.* **53** 2571
[34] Andersen O K, Pawlowska Z and Jepsen O 1986 *Phys. Rev.* B **34** 5253
[35] Andersen O K, Jepsen O and Glötzel D 1985 *Highlights in Condensed Matter Theory* ed F Bassani, F Fumi and M P Tosi (Amsterdam: North Holland) p 59
[36] Van Schilfgaarde M, Paxton A T, Jepsen O and Andersen O K 1992 unpublished
[37] Andreas Emil Kumm 1992 *PhD thesis* University of Stuttgart
[38] Jepsen O and Andersen O K 1971 *Solid State Commun.* **91** 1763
[39] Blöchl P 1989 *PhD thesis* University of Stuttgart
[40] Villars P and Calvert L D 1985 *Pearson's Handbook of Crystallographic Data for Intermetallic Phases* vol 1–3 (American Society for Metals)
[41] Brandes E A (ed) 1983 *Smithells Metals Reference Book* (Boston: Butterworths) 6th edn
[42] Barin I, Knacke O and Kubaschewski O 1977 *Thermochemical Properties of Inorganic Substances* (Berlin: Springer)
[43] Kaufman L and Bernstein H 1970 *Computer Calculation of Phase Diagrams* (New York: Academic) p 185
[44] Smith H G 1987 *Phys. Rev. Lett.* **58** 1228
[45] Moruzzi V L, Janak J F and Williams A R 1978 *Calculated Electronic Properties of Metals* (New York: Pergamon)